

# Chapter 8

## Modeling for LMSS Scenarios

### 8.1 Background

Modeling serves a variety of purposes for characterizing land mobile satellite propagation. Without the availability of data, a qualitative propagation model is desirable in order to design propagation experiments which measure important signal characteristics without imposing instrumentation limitations. Once data are available, quantitative models can be developed to explain the observed signal variations and their dependence on a wide range of experimental parameters, such as the environment topography, link elevation angle, vehicle speed, or receiver antenna pattern. As models reach maturity, they can be employed to predict system performance under specified conditions or to simulate the actual operation for LMSS scenarios with a particular choice of modulation and coding. Good models based on a thorough understanding of the causes of signal degradation can then be used as aids in optimizing system design and to explore fade mitigation strategies.

Much work has been done to characterize the signal variations observed in terrestrial land mobile propagation at UHF [Jakes, 1974; Lee, 1986]. While some of the same basic concepts of signal statistics apply also to LMSS, significant differences exist and require the development of LMSS specific models. Satellite systems are usually power limited because it is expensive and/or impractical to operate high-power transmitters and high-gain antennas in space. Such systems therefore function with relatively low fade margins at or near the

line-of-sight signal level. On the other hand, terrestrial systems can apply higher power levels and do not need to establish a line-of-sight signal path. They normally operate by utilizing the scattered multipath signals. In contrast, satellite systems must utilize the line-of-sight component for communications, and multipath scattering represents interference.

In response to the needs of experimenters and system designers, several distinct types of LMSS models have been developed. Three classes of models are described in the following paragraphs. They are classified here as: (1) empirical regression fits to data, (2) probability distribution models, and (3) geometric-analytic models. The empirical regression fits to data models describe probability distributions of fades based on experimental measurements. The second class, statistical probability distributions models, are based on the utilization of a composite of several probability density functions customarily used in radio wave propagation; namely, Rayleigh, Rician, and lognormal statistics. Among these, some combine densities based on physical reasoning about the propagation process, while others add the use of fade state or fade state transition probabilities. The third class of models employ geometrical analytical procedures for predicting the effects of single and multiple scatterers.

The choice as to which model is most appropriate depends very much on the intended application and which propagation phenomenon one wants to predict. Of the different types, empirical models do not provide insight into the physics of propagation processes, but they characterize the sensitivity of the results to important parameters. Statistical models build upon an understanding of the processes which cause signal variations, but with simplifying assumptions. Analytical models attempt to describe a particular propagation scenario deterministically, but then have to use statistics to extend the results to realistic situations.

In this chapter are described background information associated with the important elements of model development. Also described are the dominant LMSS propagation models of the above types, their input and output parameters, as well as their advantages and limitations.

## 8.2 Background Information Associated with Model Development

### 8.2.1 Diffusely Scattered Waves

To explain signal variations specific to LMSS transmissions between a satellite and a moving vehicle, the interactions of two important signal components have to be considered: line-of-sight and diffusely scattered waves. We ignore the ground reflected waves since it is presumed that for LMSS scenarios, any energy directed towards the antenna near the horizontal will be outside its beamwidth and be filtered out by the low gain pattern function values.

The direct wave may be approximated by a plane wave propagated along the line-of-sight path, with most of the power transmitted through the central few Fresnel zones. It may be completely obscured by obstacles such as mountains, buildings, or overpasses, or it may be partially shadowed by roadside trees or utility poles. The shadowing process may be explained by absorption, diffraction, scattering, or a combination thereof. The frequency of the direct wave is shifted by an amount proportional to the relative speed between the satellite and the vehicle.

A scenario for diffuse scattering for mobile reception may be described as follows. Transmissions from a satellite illuminate obstacles in the vicinity of the vehicle resulting in reflected energy emanating from multiple scatterers. Waves from these scatterers arrive at the receiving antenna with random, polarizations, amplitudes, and phase, where the individual contributions have been delayed by the amount of time corresponding to the extra path traveled. In addition, the individual contributions undergo a Doppler shift proportional to the relative speed between any particular scatterer and the vehicle. It is limited to a band of frequencies relative to the zero speed center frequency given by,

$$\Delta f_D = \pm \frac{v}{\lambda} \quad (8.1)$$

where  $v$  is the vehicle speed in m/s and  $\lambda$  is the wavelength in m. The + and - signs denote an increase and decrease of frequency assuming the illuminated obstacles are directly in front of and behind the vehicle, respectively. This, of course, represents a worst case scenario which may occur at locations where there are sharp bends in the road. As an example, a vehicle traveling at 25 m/s ( $\approx 55$  mi/h) receiving L-Band (1.5 GHz or  $\lambda = 0.2$  m), will experience Doppler shifts limited to  $\pm 125$  Hz.

### 8.2.2 Faraday Rotation

Faraday rotation effects [Davies, 1990; Flock, 1987] are potential contributors to signal strength variations which can be neglected for LMSS systems which employ circular polarization. The ionosphere contains free electrons in a relatively static magnetic field. This combination causes polarization rotation of linearly polarized waves as given by (for  $f > 100$  MHz)

$$\phi = 1.35 \times 10^6 \frac{B_e \text{ TEC}}{f^2} \quad (\text{deg}) \quad (8.2)$$

where where  $f$  is the frequency in Hz and  $B_e$  is the effective earth's magnetic field in Webers/m<sup>2</sup> defined by

$$B_e = \frac{\int N B \cos \theta_B d\ell}{\text{TEC}} \quad (8.3)$$

and where  $\theta_B$  is the angle between the direction of propagation and the earth's magnetic flux density vector. TEC is the total electron content (#/m<sup>2</sup>) given by

$$\text{TEC} = \int N d\ell \quad (\# \text{ of electrons/m}^2) \quad (8.4)$$

where  $\ell$  is the path length through the ionosphere and  $N$  (#/m<sup>3</sup>) is the electron density along the path. Assuming, extreme values of TEC and  $B_e$  given by [CCIR, 1986b (Report 263-6)],

$$\text{TEC} = 1.86 \times 10^{18} \quad (\#/m^2) \quad (8.5)$$

$$B_e = 0.43 \times 10^{-4} \quad (\text{Webers/m}^2) \quad (8.6)$$

polarization rotations of 142.7° and 48.0° occur at  $f = 870$  MHz and  $f = 1.5$  GHz, respectively. It is apparent that at UHF frequencies, significant signal loss due to polarization mismatch may occur. As mentioned, this is normally avoided by transmitting and receiving circular polarized signals since the receiving antenna is insensitive to the same polarization shifts of the orthogonal linear components comprising the circular polarized wave.

### 8.2.3 Ground Specular Reflection

This type of specular reflection is generated on the ground near the vehicle, where the ray from the reflection point to the antenna is below the horizontal. This coherent reflection

comes from an area around the intercept point the size of a few Fresnel zones. Its strength, relative phase shift, and polarization depend on the roughness and dielectric properties of the ground and are elevation angle sensitive. In a system utilizing a low-gain antenna (e.g., a dipole) which can geometrically see the specular point and also has gain in that direction, destructive interference between the specular reflection and the direct wave can produce deep fades [CCIR, 1986a (Report 1008); Flock, 1986].

The antennas contemplated for use in LMSS are either low-cost, medium gain, fixed pointed or higher-cost, high gain, tracking antennas. A typical medium gain antenna is a crossed drooping dipole, which has azimuthally omni-directional gain of about 4 dB from 15° to 60° elevation. At lower elevation angles its gain decreases rapidly, thus providing protection against both specular reflection from the ground near the vehicle as well as multipath scatter from elevated objects at larger distances. A high-gain antenna, typically a mechanically or electronically scanned array, achieves even greater rejection of multipath power and a concomitant narrowing of the Doppler spectrum. Isolation from ground specular scatter is further enhanced by placing the antenna on the center of the vehicle roof which acts as a ground plane and helps to direct the pattern upward.

Some additional rejection of the specular reflection can be achieved because circular polarization is reversed when the grazing angle of reflection is larger than the grazing Brewster angles. In particular, these grazing angles are in the range of 15° to 35° for very wet to very dry land, respectively [Reed and Russel, 1966].

### **8.3 Empirical Regression Models**

Empirical regression models correspond to fade distributions derived from experimental measurements at different frequencies, elevation angles, vehicle headings, sides of road, types of terrain, and extent of shadowing. They all have the common advantage of being based on actual data and hence they may be used with a certain degree of confidence for the prediction of fade distributions over similar types of roads. Although they are derived from "time-series" of fading events, this information is lost in the derivation of the distributions. The physics associated with the empirical models exist to the extent that the models are based on the categorized measureables, such as frequency, elevation angles, heading, and percentage of shadowing due to trees.

The common disadvantage associated with these models is that difficulties may exist in extrapolating these models to cases not considered; such as other "road-types" and frequencies outside the interval of scaling.

### 8.3.1 Large Scale - Small Scale (LS-SS) Coverage Model

The first propagation experiments targeted towards land mobile satellite communications were conducted by observing 860 MHz and 1550 MHz transmissions emanating from NASA's ATS-6 spacecraft [Hess, 1980]. Using the data base from measurements taken over about 1200 km in or near nine cities of the Western and Midwestern United States, an empirical model was derived relating the probabilities of exceeding fades for large scale (LS) and small scale (SS) "coverages." Coverage in broadcasting is defined either in terms of percentage of locations within an area or percentage of time at a particular location that there exists satisfactory service. For LMSS scenarios, signal level variations as a function of time are produced by vehicular motion. The model under discussion (denoted by LS-SS) describes statistics from measured data for small and large spatial scales. Small scale coverage (as defined by Hess) represents a driving interval of 100 m. For a vehicle speed of 25 m/s ( $\approx 55$  mi/h), this converts to a time interval of 4 seconds or the time interval of a short conversational sentence. For each 100 m interval, Hess derived a cumulative fade distribution given by

$$P_{Si}(A, A_q) = P_{Si}[A < A_q] \quad (8.7)$$

where the right hand side of (8.7) is read as "the probability that the attenuation  $A$  is smaller than a designated attenuation level  $A_q$  for the  $i$ th small scale distribution." The "large scale" distribution function  $P_L$  may be derived as follows. We first construct a large family of small scale distributions of the type depicted by (8.7) on a graph. We next intersect each of these distributions by a fixed percentage (e.g.,  $P_S = 90\%$ ) and arrive at a family of fade levels  $A_q$  from which a new cumulative fade distribution may be derived. We call this new cumulative distribution the "large scale" case and represent it by

$$P_L(A) = P_L[A < A_q | P_S] \quad (8.8)$$

The right hand side may be read as "the probability that the attenuation  $A$  exceeds a designated threshold level  $A_q$  given the condition that the small scale probability  $P_S$  assumes a particular value ( $P_S = 90\%$  for the given example). The physical significance that may be attributed to (8.8) is that it predicts the probability that the fade will be less than a

particular fade level over many kilometers of driving, assuming a given  $P_S$  which denotes the likelihood of successful reception over a 100 m driving distance.

Families of distributions of the type given by (8.7) and (8.8) were derived from data collected for different vehicle environments and path geometries. A normal distribution was fit to (8.8) from which a "mean excess path loss,  $\mu$ ," and "standard deviation,  $\sigma$ " were derived. The model equations of Hess for  $P_S = 90\%$  valid in the range of  $P_L$  from 50% to 90% are given by:

$$A(P_L) = \mu + k(P_L) \sigma \quad (8.9)$$

where

$$\mu = a_0 + a_1 \text{ ENV} + a_2 \text{ HEAD} + a_3 \text{ FREQ} + a_4 \text{ SIDE} + a_5 \text{ ELEV} \quad (8.10)$$

$$\sigma = b_0 + b_1 \text{ ENV} + b_2 \text{ HEAD} + b_3 \text{ FREQ} + b_4 \text{ SIDE} + b_5 \text{ ELEV} \quad (8.11)$$

In (8.9),  $k$  is the number of standard deviations for various values of  $P_L$  and are given by

$$k = \begin{cases} 0 & P_L = 50\% \\ 1.28 & P_L = 90\% \\ 1.65 & P_L = 95\% \\ 2.33 & P_L = 99\% \end{cases} \quad (8.12)$$

The model parameters ENV, HEAD, FREQ, SIDE, and ELEV are defined in Table 8.1. We note that the model contains the following elements: (1) the local environment (ENV), such as urban, semi-urban (commercial) and suburban, (2) the vehicle heading (HEAD) with respect to the satellite azimuth, (3) the frequency (FREQ); UHF or L-Band, (4) the side (SIDE) of the road driven (satellite located across opposing lane or not), and (5) the elevation angle (ELEV) to the satellite. The downtown area of a city, with many tall buildings and a rectangular street grid would be characterized as urban. Streets lined by shopping centers as well as by businesses with off-street parking lots are classified as commercial, and areas with small one- or two-story houses along moderately tree-lined roads define suburban environment. Data acquired in rural surroundings are included in the suburban category. The coefficients for the mean fade  $\mu$  and slope  $\sigma$  given in (8.10) and (8.11), respectively, are summarized in Table 8.2, along with their standard errors.

The overall standard errors of  $\mu$  and  $\sigma$  are

$$\text{S.E.}(\mu) = 3.65 \text{ dB} \quad (8.13)$$

Table 8.1: Parameter Definition and Values for Hess Model

Parameter	Range of Values
ENVironment	1 = Urban, 0 = Commercial, -1 = Suburban/Rural
HEADing	$-\cos 2(Az_{\text{vehicle}} - Az_{\text{satellite}})$
FREQuency	1 = UHF, 1.8 = L-Band
SIDE of road	+1=Satellite across road, -1=On same side
ELEVation	15° to 50°

$$\text{S.E.}(\sigma) = 2.5 \text{ dB} \quad (8.14)$$

In order to extend the small-scale coverage from the modeled value of  $P_S = 90\%$  as given by (8.9)-(8.11) and Table 8.2 to other values of  $P_S$ , we use the following formulation:

#### Urban and Commercial

$$A(P_L, P_S) = \begin{cases} (P_S - 90) \times 0.6 + A(P_L) & 95\% \geq P_S \geq 90\% \\ (P_S - 90) \times 0.2 + A(P_L) & 50\% \leq P_S < 90\% \end{cases} \quad (8.15)$$

#### Suburban-Rural

$$A(P_L, P_S) = (P_S - 90) \times 0.1 + A(P_L) \quad 50\% \leq P_S \leq 95\% \quad (8.16)$$

Table 8.2: Coefficients In LS-SS Fade Model

Mean Fade, $\mu$			Standard Deviation, $\sigma$		
Coeffic.	Value (dB)	Std Error (dB)	Coeffic.	Value (dB)	Std Error (dB)
$a_0$	9.55		$b_0$	3.75	
$a_1$	4.46	0.42	$b_1$	2.62	0.29
$a_2$	3.41	0.61	$b_2$	0.98	0.42
$a_3$	1.66	0.91	$b_3$	0.046	0.62
$a_4$	-0.35	0.36	$b_4$	-0.24	0.25
$a_5$	-0.052	0.045	$b_5$	0.04	0.031

**Example: LS-SS Model**

To illustrate the procedures by which we execute the LS-SS model, consider the following example. Assume that a receiver can recover the LMSS coded errors as long as the small-scale coverage is at least  $P_S = 70\%$ . The system operates at L-Band in a suburban area with an elevation angle to the satellite of  $45^\circ$ . It is desired to determine the required fade margin to achieve a large scale probability of  $P_L = 95\%$ .

We assume a worst case heading and condition of roadside, with the satellite at a right angle to and right of the vehicle. Hence, we employ the following parameter values from Table 8.1:

$$\begin{aligned} \text{ENV} &= -1 \quad (\text{Suburban/Rural}) \\ \text{HEAD} &= +1 \quad (\text{az}_{\text{vehicle}} - \text{az}_{\text{satellite}} = 90^\circ) \\ \text{FREQ} &= 1.8 \quad (\text{L - Band}) \\ \text{SIDE} &= -1 \quad (\text{Satellite Same Side}) \\ \text{ELEV} &= 45^\circ \end{aligned} \tag{8.17}$$

Substituting the above into (8.10) and (8.11), we obtain

$$\mu = 9.5 \text{ dB} \tag{8.18}$$

$$\bar{\sigma} = 4.23 \text{ dB} \tag{8.19}$$

Substituting (8.18), (8.19) and  $k = 1.65$  (from (8.12) for  $P_L = 95\%$ ) into (8.9) results in

$$A = 16.5 \text{ dB} \quad P_S = 90\% \tag{8.20}$$

The fade given by (8.20) corresponds to a large scale probability of  $P_L = 95\%$  and small scale probability of  $P_S = 90\%$ . To convert the above to the desired small scale probability  $P_S = 70\%$ , substitute (8.20) into (8.16). Hence,

$$A = 14.5 \text{ dB} \quad P_S = 70\% \tag{8.21}$$

An estimate of the standard deviation associated with (8.20) may be derived by substituting (8.13) for  $\mu$  and (8.14) for  $\sigma$  in (8.9) and calculating the square root of the sum of the squares of each of the terms (with  $k = 1.65$ ). This gives a prediction error of 5.5 dB.

In Figure 8.1 is given a family of curves of the large-scale cumulative distributions  $P_L$  for elevation angles of  $20^\circ$ ,  $30^\circ$ , and  $45^\circ$  with small-scale probabilities of  $P_S = 90\%$ ,  $70\%$ , and

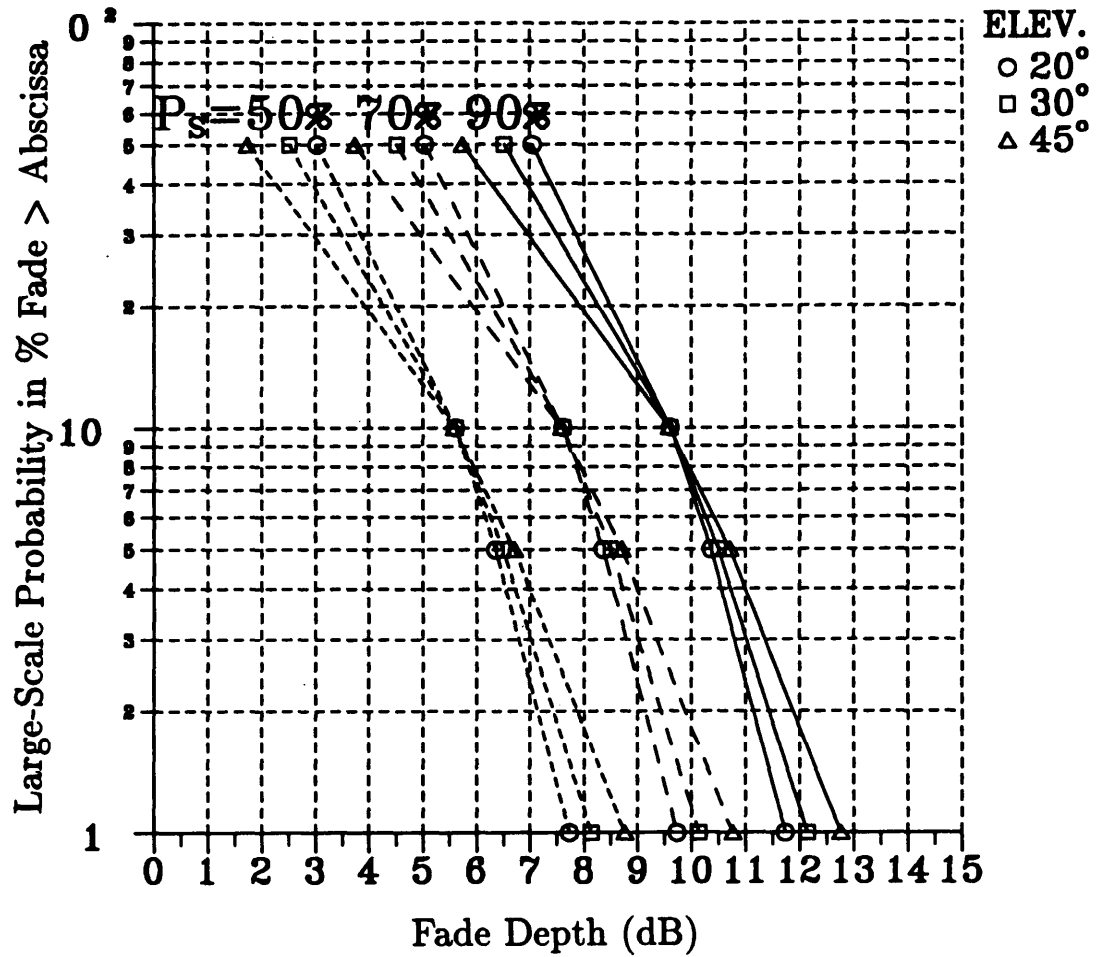


Figure 8.1: Probability distributions for LS-SS model for family of elevation angles and indicated small scale probabilities  $P_s$ .

50%. These depict an overall driving condition as each curve represents the average of four distributions; right side of road, left side of road, and difference in vehicle-satellite azimuth directions of  $90^\circ$  and  $0^\circ$ . We note that  $P_L$  is relatively insensitive to elevation angle but is highly sensitive to  $P_S$ .

### **Discussion**

The LS-SS model of Hess is derived from an extensive data base of measurement results, which is especially weighted for urban to suburban environments. It is simple to use and has realistic parameterization for the most important environmental variables.

The model was derived from data taken with linearly polarized quarter wavelength whip antennas. Such a system will not provide isolation from ground specular reflections as do low gain LMSS type antennas previously described. While shadowing loss measurements were not affected by the antenna choice, multipath and specular effects were most likely enhanced. This may have caused overprediction of signal variations especially in open rural areas where shadowing is statistically less significant than multipath. It is also important to note that the experiment emphasized urban over rural areas, making predictions from the data base for rural areas less reliable.

### **8.3.2 Empirical Roadside Shadowing Model**

Since the empirical roadside shadowing model was addressed in Section 3.3, the model details will not be described here. A short summary discussion is presented in the following paragraphs.

### **Discussion**

The ERS model is based on extensive measurements in rural and suburban environments in central Maryland using a realistic LMSS antenna comprised of a crossed drooping dipole (previously described). The model is based on systematically repeated measurements (at UHF and L-Band) along the same system of roads at different elevation angles ranging from  $20^\circ$  to  $60^\circ$ . The fade distributions are simple to calculate. They are a manifestation of an

overall average fade condition for both left and right side driving and various degrees of roadside shadowing (55% to 75%). It has been independently validated to within a few dB employing measurements in Australia.

Because of the limited dynamic range of the measurements, only the median distribution of many 90 second intervals could be determined and modeled. The higher percentile distributions (e.g., 90th or 95th) were beyond the measurement range of the equipment in the 20% to 1% range of fade exceedance. The variability of the distributions could therefore not be modeled. As is the case with the LS-SS model, the ERS model does not provide information about fade dynamics and therefore cannot be used to generate simulated data. This model is also biased in favor of the geometric condition where maximum shadowing occurs; namely, the line-of-sight path is dominantly directed perpendicular to the line of roadside trees. The model is only valid in the range of elevation angles  $20^\circ$  to  $60^\circ$ .

## **8.4 Probability Distribution Models**

Probability functions used to describe LMSS propagation are the Rayleigh and Rician for multipath effects and the lognormal for shadowing. These statistics are useful to the extent that they accurately describe the shadowing and multipath scenarios.

Models of these type correspond to homogeneous cases for which line-of-sight fading and multipath are simultaneously present, or only multipath is present under the conditions of no shadowing or complete blockage. They do not account for scenarios in which the vehicle may pass from shadowing to non-shadowing conditions (causing bursts of fading and non-fading) typical at higher elevation angles (e.g.,  $45^\circ$ ) in rural and suburban environments.

Their usefulness is also based on the ability to tailor parameters of the distributions to actual measurements. The parameters of importance are standard deviation, mean, percentage of shadowing, and ratio of line of sight to multipath power. These parameters are however tuned to "light" or "heavy" shadowing, "zero to frequent" percentage of shadowing, and "urban", "suburban", or "highway scenes." They represent a "rough" tuning to the model which is based on measurements at fixed elevation angles. It is, for example, difficult to relate these models to other elevation angles which are known to critically influence fading. Furthermore, it is difficult to extract from these statistics "time-series" of fading events for simulation purposes without the employment of experimental data.

In the following section is given an overview of the density functions used in modeling procedures. A further characterization is given by the CCIR [CCIR, 1986a (Report 1007)].

### 8.4.1 Density Functions Used In Propagation Modeling

#### Rician or Nakagami-Rice Density Function

The voltage phasors from all the reflection sources can be combined into two independent orthogonal vectors  $x$  and  $y$ , the in-phase and quadrature components, having normal envelopes and uniform phase distributions. When received together with a direct signal voltage  $a$ , the two-dimensional probability density of the received voltage can be expressed as

$$f_{xy}(x, y) = \frac{1}{2\pi\sigma^2} \exp\left[-\frac{(x-a)^2 + y^2}{2\sigma^2}\right] \quad (8.22)$$

where  $\sigma$  is the standard deviation of the voltage. The signal envelope represents the length of the voltage vector  $z$ . It is given by

$$z = \sqrt{x^2 + y^2} \quad (8.23)$$

from which we derive the Rician density  $f_z(z)$  [Papoulis, 1965]

$$f_z(z) = \frac{z}{\sigma^2} \exp\left[-\frac{(z^2 + a^2)}{2\sigma^2}\right] I_0\left(\frac{za}{\sigma^2}\right) \quad (8.24)$$

where  $I_0$  is the zeroth order modified Bessel function.

The normalized line-of-sight power is given by

$$P'_{los} = \frac{a^2}{2} \quad (8.25)$$

and the average (normalized) multipath power is given by

$$P'_{mp} = \sigma^2 \quad (8.26)$$

where we denote the powers by a prime to distinguish it from probability. The ratio of these two powers defines the  $K$  value which characterizes the influence of multipath scattering on the signal distribution. Hence,

$$K = \frac{P'_{los}}{P'_{mp}} = \frac{a^2}{2\sigma^2} \quad (8.27)$$

Usually, the K factor is quoted in terms of dB. That is,

$$K(\text{dB}) = 10 \log \left( \frac{P'_{\text{los}}}{P'_{\text{mp}}} \right) = 10 \log \left( \frac{a^2}{2\sigma^2} \right) \quad (8.28)$$

It is apparent from (8.27) that the lower the relative level of the multipath power, the larger the K value, and conversely. Further normalizing  $P'_{\text{los}}$  such that  $P'_{\text{los}} = 1$ , reduces the Rician density (8.24) to a single parameter density function of the voltage, which can be written as a function of K by

$$f_z(z) = K z \exp \left[ -K \left( \frac{z^2}{2} + 1 \right) \right] I_0(Kz\sqrt{2}) \quad (8.29)$$

where

$$K = \frac{1}{\sigma^2} \quad (8.30)$$

### Rayleigh Density Function

The Rayleigh density is a special case of the Rician distribution and arises when no line-of-sight power is received. Setting  $a = 0$  in (8.24)

$$f_z(z) = \frac{z}{\sigma^2} \exp \left( -\frac{z^2}{2\sigma^2} \right) \quad (8.31)$$

Even though no direct signal is received, the Rayleigh density can also be defined in terms of a  $\bar{K}$ -factor

$$\bar{K} \equiv \frac{1}{\sigma^2} \quad (8.32)$$

Substituting (8.32) into (8.31)

$$f_z(z) = \bar{K} z \exp \left( -\bar{K} \frac{z^2}{2} \right) \quad (8.33)$$

Note that the Rayleigh distribution has but a single parameter (namely,  $\sigma$  or  $\bar{K}$ ). For Rayleigh scattering, the average scattered power is variable, but the standard deviation on a dB scale is constant and equal to 5.57 dB. As a rule of thumb, based on the Central Limit Theorem [Papoulis, 1965], at least six random scattering sources are required to produce a Rayleigh (or Rician) distribution.

### Lognormal Density Function

Shadowing is a manifestation of the absorption and scattering of the incident direct wave by roadside trees or other obstacles as it is transmitted via the line-of-sight between the satellite and the vehicle. The cumulative distribution function of the received power expressed in dB can often be fit to a straight line when plotted on a normal probability scale. The voltage variation due to shadowing is then lognormal. The lognormal density function for a random variable  $z$  can be derived from the normal density function for  $x$  by using

$$x = \ln(z). \quad (8.34)$$

In this case the lognormal density of  $z$  has the form

$$f_z(z) = \frac{1}{sz\sqrt{2\pi}} \exp \left[ -\frac{(\ln(z) - m)^2}{2s^2} \right] \quad (8.35)$$

where  $m$  and  $s$  are the mean and standard deviation of  $\ln(z)$ , respectively. Since the power ( $x$ ) is usually expressed in dB, the relation between  $x$  (in dB) and  $z$  is

$$x = 10 \log(z) \quad z = \text{power (watts)} \quad (8.36)$$

or

$$x = 20 \log(z) \quad z = \text{voltage (volts)} \quad (8.37)$$

The lognormal density function of power when  $z$  is the power in watts is

$$f_z(z) = \frac{4.343}{sz\sqrt{2\pi}} \exp \left[ -\frac{(10 \log(z) - m)^2}{2s^2} \right] \quad z = \text{power (watts)} \quad (8.38)$$

where  $m$  and  $s$  are the mean and standard deviation of  $10 \log(z)$ , respectively. The lognormal density function of power when  $z$  is voltage is

$$f_z(z) = \frac{8.686}{sz\sqrt{2\pi}} \exp \left[ -\frac{(20 \log(z) - m)^2}{2s^2} \right] \quad z = \text{voltage (volts)} \quad (8.39)$$

where  $m$  and  $s$  are the mean and standard deviation of  $20 \log(z)$ , respectively.

### 8.4.2 Loo's Distribution Model

A statistical model for land mobile satellite propagation based on probability density functions of multipath and shadowing propagation has been developed by Loo [1985; 1987]. The following assumptions are made: (a) the receiver voltage due to the diffusely scattered power is Rayleigh distributed, and (b) the voltage variations due to attenuation of the line-of-sight signal are lognormally distributed. The two voltages are considered correlated, as attenuation by trees is caused by both absorption and scattering, some of the latter directed into the receiver. The model employs the parameters  $\bar{K}$  as given by (8.32), as well as the mean  $m$  and standard deviation  $s$  previously defined for lognormal fading. The mean scattered power in the model is set constant at a level that depends on the severity of the shadowing relevant to a particular environment. While the line-of-sight attenuation is constant, a conditional Rician distribution of the signal envelope holds. The overall probability density is found by integration of the conditional density multiplied by the lognormal probability of the line-of-sight envelope. The resulting probability density function of the signal envelope is

$$f_v(v) = \frac{\bar{K}v}{s\sqrt{2\pi}} \int_0^\infty \frac{1}{z} \exp \left[ -\frac{(\ln(z) - m)^2}{2s^2} - \frac{\bar{K}(v^2 + z^2)}{2} \right] I_0(\bar{K}vz) dz \quad (8.40)$$

For signal voltages much greater and much less than the standard deviation of the Rayleigh process, the density function is lognormal or Rayleigh, respectively, and can be simplified to

$$f_v(v) = \frac{1}{sv\sqrt{2\pi}} \exp \left[ -\frac{(\ln(v) - m)^2}{2s^2} \right] \quad v \gg \frac{1}{\sqrt{\bar{K}}} \quad (8.41)$$

and

$$f_v(v) = \bar{K}v \exp \left( -\frac{\bar{K}v^2}{2} \right) \quad v \ll \frac{1}{\sqrt{\bar{K}}} \quad (8.42)$$

At intermediate values of  $v$ ,  $f_v(v)$  is found by numerical integration.

Table 8.3: Parameters for Loo's Model

Shadowing Class	Rayleigh Scatter	Lognormal Shadowing	
	$\bar{K}$	m	s
Infrequent light	6.3	0.115	0.115
Frequent heavy	15.8	-3.91	0.805
Overall	4.0	-0.69	0.23

The probability that the received voltage is less than or equal to  $v$  is

$$F_v(v) = \int_0^v f_v(u) du \quad (8.43)$$

from which the cumulative distribution function  $A$  in dB is found using

$$A = 20 \log(v) \quad (8.44)$$

Values of the model parameters were derived by Loo from propagation data measured over a helicopter to vehicle link with  $15^\circ$  elevation angle in a rural environment with two classes of shadowing: infrequent light and frequent heavy. The parameters are summarized in Table 8.3.

### Level Crossing Rate and Average Fade Duration

In addition to describing the fade cumulative distribution function, Loo's model also provides insight into the dynamics of fading by deriving statistical relations for the level crossing rate

(LCR) and the average fade duration (AFD). The level crossing rate is the expected rate at which the signal envelope crosses a specified signal level with a positive slope. The average fade duration is the expected time or distance the signal envelope is below the specified signal level. The inverse of the level crossing rate is the sum of the average fade and non-fade durations. The derivation, based on earlier work by Rice and Jakes, hinges on the statistical independence between the signal envelope and its time derivative, which is assumed to be a Gaussian process both for Rician and lognormal fading. The LCR is normalized by the maximum possible Doppler shift

$$f_{\max} = \frac{v}{\lambda} \quad (8.45)$$

where  $v$  is the vehicle speed and  $\lambda$  is the wavelength. The normalized level crossing rate  $\text{LCR}_n$  is based on the wavelength, independent of speed, and can be written as

$$\text{LCR}_n = \frac{\text{LCR}}{f_{\max}} = \sqrt{2\pi} \sqrt{(1 - \rho^2)} \sigma^2 \frac{\sqrt{\sigma^2 + 2\rho\sigma s + s^2}}{\sigma^2 (1 - \rho^2) + 4\rho\sigma s} f_v(v) \quad (8.46)$$

where  $\rho$ , now a fourth parameter of Loo's model, is the correlation coefficient for the rate of change of the envelope due to multipath and shadowing effects. Typically, the correlation coefficient  $\rho$  was in the range from 0.5 to 0.9 for the data set used by Loo.

The AFD can be found from  $\text{LCR}_n$  by

$$\text{AFD} = \frac{1}{\text{LCR}_n} \int_0^L f_v(v) dv \quad (8.47)$$

With supporting helicopter data at 870 MHz and satellite data at 1542 MHz and for elevation angles from 5° to 30°, it was shown that the signal phase and the rate of change of the phase can be treated as Gaussian processes [Loo, 1987]. Values of the mean and standard deviation were 7.5° and 12.6° at 870 MHz, and 7.5° and 26° at 1542 MHz, respectively.

## Discussion

The Loo model provides a description of primary and secondary fade statistics for LMSS scenarios based on four parameters derived from measurements performed in Canada. As all of the measurements were made at elevation angles below 30°, model parameters for higher elevation angles are not available.

### 8.4.3 Total Shadowing Model

Another statistical model characterizing the fade distribution applicable to LMSS propagation has been devised by Lutz et al. [1986]. As in Loo's model, Rician, Rayleigh, and lognormal probability densities are combined and model parameters are derived from least-square error fits to measured data. However, there are significant differences in the way the three distributions are assigned to the two major propagation phenomena, scattering and shadowing. As described in the previous section, Loo combines a constant intensity Rayleigh distributed scattering voltage with a lognormally shadowed line-of-sight signal voltage. Lutz et al., on the other hand, consider two distinct propagation link states; shadowing, and no shadowing. In the unshadowed state, the envelope statistics are assumed to be Rician with constant K-factor due to the superposition of the direct wave with constant intensity multipath echoes. When the propagation link is shadowed by roadside trees, the line-of-sight is assumed to be totally obscured and most of its power converted into scattered waves, leaving only multipath signals with Rayleigh statistics, but their average strength is modeled as lognormally distributed. Loo modulates the Rician K-factor by shadowing the line-of-sight component. Lutz, in the shadowed state, varies the intensity of the Rayleigh scattering process, or the  $\bar{K}$  factor, in the absence of any line-of-sight signal. In Lutz's model, the probability density of the received voltage for the unshadowed fraction (1-S) of the driving distance is Rician. When expressed in terms of the received power  $P'$ , it has the form

$$f_{P',\text{Rice}}(P') = K \exp[-K(P' + 1)] I_0(2K\sqrt{P'}) \quad (8.48)$$

where unity line-of-sight power is assumed and  $K$  is the ratio of line-of-sight to average multipath power. That is

$$K = \frac{1}{P'_{\text{mp}}} \quad (8.49)$$

For the shadowed fraction  $S$  of the total distance, it is Rayleigh distributed and has the following form when expressed in terms of the received power,  $P'$

$$f_{P',\text{Rayleigh}}(P') = \bar{K} \exp(-\bar{K} P') \quad (8.50)$$

where  $\bar{K}$  is the reciprocal of the average multipath power as given by (8.32). Lutz et al. postulate this multipath power Rayleigh intensity  $1/\bar{K}$  to be lognormally distributed. The

density can be expressed in terms of the  $\bar{K}$ -factor, the mean  $m$ , and the standard deviation  $s$  of  $10 \log(\bar{K})$  as

$$f_{\bar{K}}(\bar{K}) = \frac{4.343}{\bar{K} s \sqrt{2\pi}} \exp \left[ -\frac{(10 \log(\bar{K}) - m)^2}{2 s^2} \right] \quad (8.51)$$

where

$$m = E [10 \log(\bar{K})] \quad (8.52)$$

and

$$s = \left\{ E \left[ (10 \log(\bar{K}))^2 \right] - m^2 \right\}^{1/2} \quad (8.53)$$

where  $E$  denotes the "expected value."

The overall probability density of the received power follows by combining (8.48) and (8.50) with (8.51)

$$f_{P'}(P') = (1 - S) f_{P', \text{Rice}}(P') + S \int_0^{\infty} f_{P', \text{Rayleigh}}(P' | \bar{K}) f_{\bar{K}}(\bar{K}) d\bar{K} \quad (8.54)$$

The cumulative distribution of the fractional distance the fade exceeds  $A$  dB is found by evaluating (8.54). Model parameters were determined by Lutz et al. from regressions to satellite measurements performed in various environments with a  $24^\circ$  elevation angle. They are summarized in Table 8.4 for a vehicle antenna with a hemispherical pattern. Good fits of the model to the measured cumulative distribution functions of the attenuation were obtained.

### Discussion

The Lutz et al. experiments were carried out using three different receiving antennas. The shadowing parameter  $S$  derived from the corresponding data sets was found to be dependent on the antenna, which indicates a coupling of  $S$  to multipath propagation. Had the model been a true representation of LMSS propagation,  $S$  should have been independent of the antenna pattern.

Table 8.4: Typical Parameters for Total Shadowing Model of Lutz et al. [1986]

Environment	S	K(dB)	m(dB)	s(dB)
Urban	0.60	3.0	-10.7	3.0
Suburban	0.59	9.9	-9.3	2.8
Highway	0.25	11.9	-7.7	6.0

#### 8.4.4 Lognormal Shadowing Model

Smith and Stutzman [1986] incorporated the idea into a model that different statistics should be used to describe LMSS signal variations depending on whether the propagation path is shadowed or unshadowed. They developed a model which assigns Rayleigh, Rician and lognormal behavior of the received signal voltage in a manner similar to Loo's model. In the unshadowed state, the received signal consists of the sum of the direct signal and a constant average intensity Rayleigh voltage due to the diffusely scattered multipath echoes. The resulting signal amplitude has a Rician probability density characterized by a constant ratio of direct to scattered power. In the shadowed state, the amplitude of the line-of-sight signal is assumed to have lognormal statistics. When combined with constant level diffuse multipath, the probability density (8.40) derived by Loo applies.

The overall probability density of the received voltage is developed in analogy to the derivation of (8.54) as

$$\begin{aligned}
 f_v(v) = & (1 - S) K v \exp \left[ -K \left( \frac{v^2}{2} + 1 \right) \right] I_0(K v) + S \frac{8.686 \bar{K} v}{s \sqrt{2\pi}} \\
 & \times \int_0^\infty \frac{1}{z} \exp \left[ \frac{-(20 \log(z) - m)^2}{2 s^2} - \frac{\bar{K} (v^2 + z^2)}{2} \right] I_0(\bar{K} v z) dz \quad (8.55)
 \end{aligned}$$

where S, K,  $\bar{K}$ , m, and s are the five model parameters already described in the previous

density can be expressed in terms of the  $\bar{K}$ -factor, the mean  $m$ , and the standard deviation  $s$  of  $10 \log(\bar{K})$  as

$$f_{\bar{K}}(\bar{K}) = \frac{4.343}{\bar{K} s \sqrt{2\pi}} \exp \left[ -\frac{(10 \log(\bar{K}) - m)^2}{2 s^2} \right] \quad (8.51)$$

where

$$m = E [10 \log(\bar{K})] \quad (8.52)$$

and

$$s = \left\{ E \left[ (10 \log(\bar{K}))^2 \right] - m^2 \right\}^{1/2} \quad (8.53)$$

where  $E$  denotes the "expected value."

The overall probability density of the received power follows by combining (8.48) and (8.50) with (8.51)

$$f_{P'}(P') = (1 - S) f_{P', \text{Rice}}(P') + S \int_0^{\infty} f_{P', \text{Rayleigh}}(P' | \bar{K}) f_{\bar{K}}(\bar{K}) d\bar{K} \quad (8.54)$$

The cumulative distribution of the fractional distance the fade exceeds  $A$  dB is found by evaluating (8.54). Model parameters were determined by Lutz et al. from regressions to satellite measurements performed in various environments with a  $24^\circ$  elevation angle. They are summarized in Table 8.4 for a vehicle antenna with a hemispherical pattern. Good fits of the model to the measured cumulative distribution functions of the attenuation were obtained.

### Discussion

The Lutz et al. experiments were carried out using three different receiving antennas. The shadowing parameter  $S$  derived from the corresponding data sets was found to be dependent on the antenna, which indicates a coupling of  $S$  to multipath propagation. Had the model been a true representation of LMSS propagation,  $S$  should have been independent of the antenna pattern.

### 8.4.5 Simplified Lognormal Shadowing Model

This model [Barts and Stutzman, 1991; Bartz et al., 1987] has the inputs  $K$ ,  $\bar{K}$ ,  $m$ ,  $s$ , and  $S$  which have been defined in the previous two sections and assume the values summarized in Table 8.5. The resultant probability distribution model is expressed in terms of the contributions for the "no shadowing" and "shadowing" cases in the following way

$$P(A > A_q) = P_{ns} (1 - S) + P_s S \quad (8.56)$$

where  $P_{ns}$  is the probability distribution for the case of no shadowing of the line of sight and is given by,

$$P_{ns}(A > A_q) = \exp \left[ -\frac{(A + U_1)}{U_2} \right] \quad (8.57)$$

where the parameters  $U_1$  and  $U_2$  are functions of  $K$  and are given by

$$U_1 = 0.01 K^2 - 0.378 K + 3.98 \quad (8.58)$$

$$U_2 = 331.35 K^{-2.29} \quad (8.59)$$

In (8.56),  $P_s$  is the probability distribution for the case of shadowing of the line of sight and is

$$P_s(A > A_q) = (50 - A_q) \frac{V_2}{V_1} \quad (8.60)$$

where the parameters  $V_1$  and  $V_2$  are given by the following functions of  $\bar{K}$  as well as the mean  $m$  and standard deviation  $s$  of the lognormal signal

$$V_1 = -0.275 \bar{K} + 0.723 m + 0.336 s + 56.979 \quad (8.61)$$

$$V_2 = (-0.006 \bar{K} - 0.008 m + 0.013 s + 0.121)^{-1} \quad (8.62)$$

Typical fade predictions calculated from (8.56) have been plotted in Fig. 8.2 for light and heavy as well as in Fig. 8.3 for medium heavy shadowing, for infrequent ( $S=0.25$ ), moderate ( $S=0.5$ ) and frequent ( $S=0.75$ ) shadowing occurrences. In the worst case scenario: heavy and frequent shadowing, the calculated fade probabilities may exceed 1.0, but should be limited to that value.

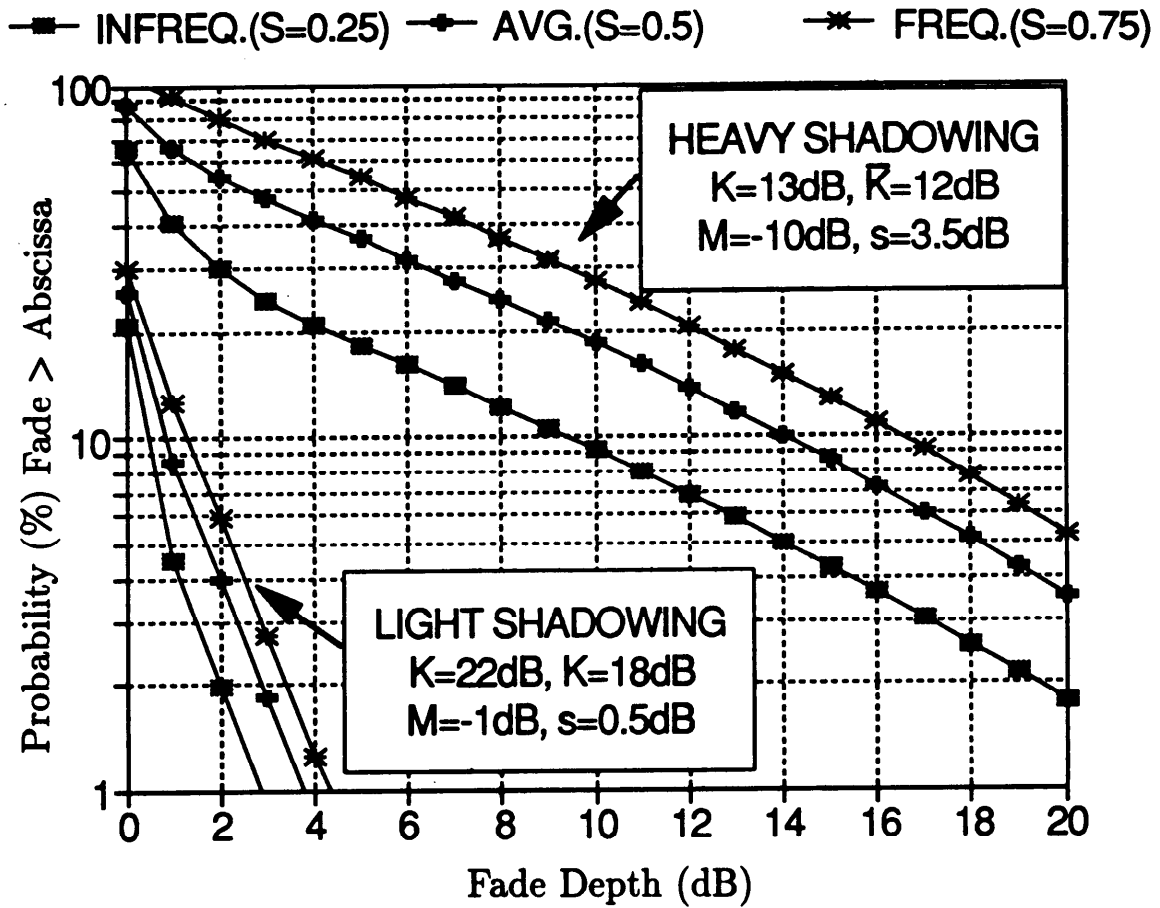


Figure 8.2: Typical fade distributions calculated from the Simplified Lognormal Shadowing Model for light (L), and heavy (H) shadowing, and for infrequent (I;  $S = 0.25$ ), moderate (M;  $S = 0.5$ ), and frequent (F;  $S = 0.75$ ) shadowing occurrences.

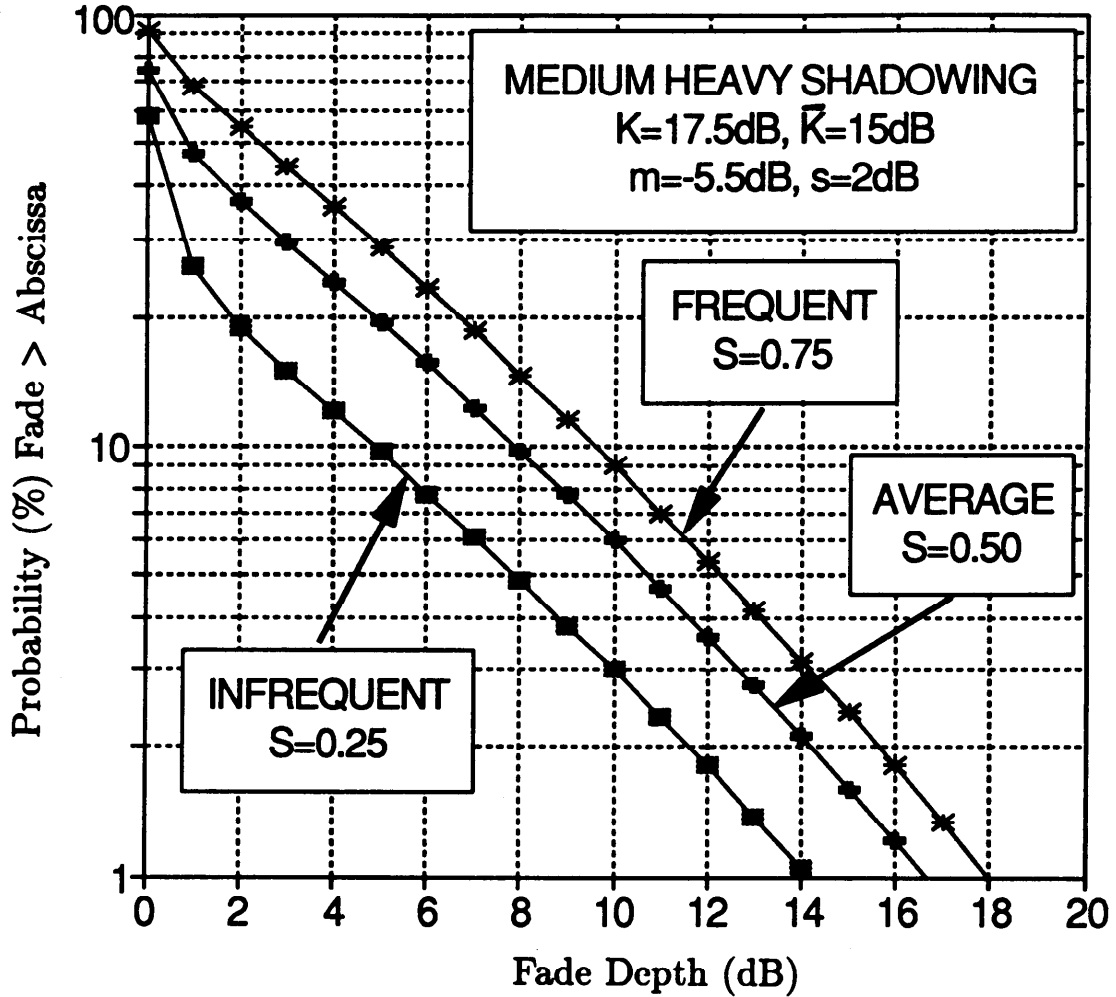


Figure 8.3: Typical fade distributions calculated from the Simplified Lognormal Shadowing Model for medium shadowing (M), and for infrequent (I;  $S = 0.25$ ), moderate (M;  $S = 0.5$ ), and frequent (F;  $S = 0.75$ ) shadowing occurrences.

### Discussion

The model has been shown to fit measured fade distributions when the propagation parameters were determined by tailoring the data to the model. Calculation procedures are straightforward.

### 8.4.6 Models With Fade State Transitions

#### Two- and Four-State Markov Modeling

A 2-state Markov model (Gilbert-Elliot model) for non-shadowed (good) and shadowed (bad) channel conditions and a 4-state Markov model, also with good and bad states and qualified by either short or long duration, have been used to predict error rates in the land mobile satellite channel [Cygan et al., 1988]. Channel states are related to the presence or absence of shadowing conditions and both models describe the transition probabilities between states. Model parameters are determined from data collected in L-Band satellite propagation experiments carried out in a variety of environments at elevation angles between 21° and 24°. The data set on which the parameters are based is the same as the one used for the derivation of the total shadowing model.

The 2-state model has a total of four parameters, of which two are signal level dependent error rates and two are state transition probabilities. A summary of its parameters for three propagation scenarios is given in Table 8.6. The derived bad lengths appended to the table may be reasonable in the urban environment where much of the shadowing is due to blockage by buildings. For tree shadowing prevalent in the suburban environment, the 2-state model is lacking in predicting the effects of many short fades observed in real channel measurements.

At the price of being more calculation intensive, the 4-state model is capable of providing a more realistic statistical simulation of error bursts. It has a total of thirteen parameters, of which eight are state transition probabilities, two express the transitional durations between short and long good or bad states, and three are measures for the error probabilities in all good and short and long bad states. Typical values of the transitional durations for good/bad states are 0.46/1.85 m for urban, 0.92/0.65 m for suburban, and 5.2/2.5 m for highway driving, respectively. Error probabilities range from  $1 \times 10^{-4}$  –  $3.5 \times 10^{-4}$  for the good states to 0.16 – 0.37 for the bad states, with the short bad state's error rate about 30%

Table 8.6: Parameters for 2-State Model

Parameter	Remark	Urban	Suburban	Highway
$P_{GB}$	Transition probability from "good" to "bad" state	$3.95 \times 10^{-4}$	$2.1 \times 10^{-4}$	$2.96 \times 10^{-5}$
$P_{BG}$	Transition probability from "bad" to "good" state	$1.05 \times 10^{-4}$	$1.54 \times 10^{-4}$	$1.29 \times 10^{-4}$
$\epsilon_G$	Error rate in "good" state	$2.1 \times 10^{-4}$	$3.4 \times 10^{-4}$	$1.1 \times 10^{-4}$
$\epsilon_B$	Error rate in "bad" state	0.317	0.298	0.194
$L_G$	Derived "good" length (m)	24	45	704
$L_B$	Derived "bad" length (m)	88	60	161

below the long bad state. While the discussion of error probabilities is beyond the scope of this text, these models give an indication of the level of complexity that may be required for successfully modeling the LMSS channel.

### **Markov Transitions, Multipath, and Fade Depth Model**

By combining three distinct concepts into one LMSS propagation model, Wakana [1991] has modeled fading and its spatial characteristics. Fading due to multipath is rendered by Rician statistics (8.29), while fading of the line-of-sight signal due to tree shadowing is described in terms of a Markov model for the transitions between fade states and an attenuation algorithm for the fade depth. Like the 4-state model described above, this Markov model considers transition probabilities between four fade states: fade or non-fade, short or long, but with a total of only six as opposed to eight independent parameters. Of two attenuation models introduced, one linking the attenuation to the fade state, the other to the fade duration, the former alternative was used. Besides the six state transition probabilities, four other parameters are required. They are the Rician K-factor for the multipath scattering, attenuation levels for short and long fades, and a lowpass filter time constant to smooth the transitions between fade and non-fade states. The ten model parameters were determined for one particular suburban propagation path geometry with an optimization procedure performed on data collected in a helicopter experiment. Simulated data produced using these parameters are qualitatively similar to real data when time series are compared and have, of course, similar cumulative distributions of fades, fade durations, and non-fade durations. Typical parameter values are in the range of 0.13 – 0.97 for the transition probabilities, 10.7 dB attenuation for both fade states, a 13 dB K-factor, and a 22 Hz lowpass filter cut-off frequency, corresponding to a spatial filter of about 1 m.

Variations of the signal level at near line-of-sight power, which may be due to diffraction at the fade state transition zone and specular reflection from the ground near the vehicle have not been considered in the model development and therefore are not replicated by the simulator. Until parameters are determined for a variety of environments and elevation angles, the modeling results cannot readily be applied to other propagation geometries.

## 8.5 Geometric Analytic Models

Geometric analytic models are useful for gaining physical insight of the mechanism of fading and characteristics of signal retrieval. They may also be used to achieve time-series fades which may be interfaced with simulation techniques. Unfortunately, the complexities of "real life" scenarios do not lend themselves to analytic models and only simplified and idealized scenarios are considered.

### 8.5.1 Single Object Models

#### Point Scatterer Multipath

Frequently, signal variations observed in satellite land-mobile propagation experiments can be correlated with the receiving vehicle passing in the vicinity of a generator of multipath scattering, such as a utility pole or roadside sign. To increase understanding of these multipath reflections observed from a moving platform, a physical model based on the geometry of a single point scatterer has been developed [Vogel and Hong, 1988]. While the model does not address the major limitation of LMSS, shadowing, it provides a tool to study the dependence of signal variations observed under clear line-of-sight conditions on parameters such as antenna pattern, path azimuth and elevation angles, distance of multipath sources, and bandwidth.

A sketch of the propagation scenario considered is shown in Fig. 8.4, in which a vehicle carries an antenna with a given pattern along the x-axis with speed  $v$ . A plane wave transmitted from a satellite propagates into the direction  $(\Theta_t, \Phi_t)$ . In addition to the line-of-sight wave, the vehicle also receives one multipath component scattered by an object at  $(x_s, y_s, z_s)$ . The vectorial sum of the two waves constitutes the received signal. In order to achieve simplicity in the numerical evaluation of the model, the following assumptions were made: 1) there is only one scatterer, 2) it scatters isotropically, and 3) the receiving antenna's gain is azimuthally omnidirectional. The formula developed by Vogel and Hong [1988] for the received electric field strength  $E_r$  is

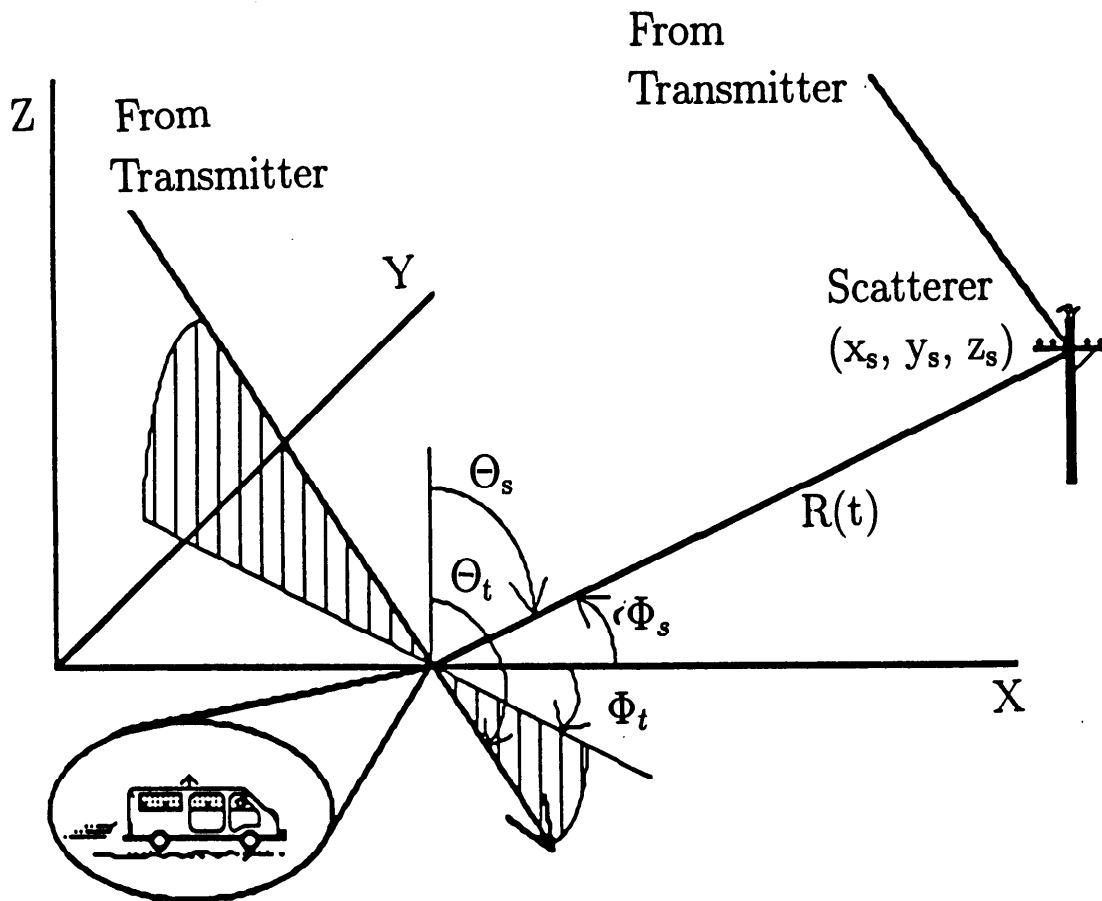


Figure 8.4: Propagation geometry for single object scattering in which a vehicle traveling at a speed  $v$  carries an antenna with a given pattern along the x-axis

$$E_r(t) = E_o D(\Theta_t) \exp [j\omega_o t - \beta] \times \left\{ T + \frac{\sqrt{\sigma} D(\Theta_s)}{2\sqrt{\pi} R(t) D(\Theta_t)} \exp \left[ j \frac{2\pi}{\lambda} (a(t) - p - R(t)) \right] \right\}, \quad (8.63)$$

where  $\beta$  is the phase shift given by

$$\beta = \frac{2\pi}{\lambda} vt \sin(\Theta_t) \cos(\Phi_t), \quad (8.64)$$

$a(t)$  is the path length from the wave through the origin to the antenna given by

$$a(t) = t \sin(\Theta_t) \cos(\Phi_t), \quad (8.65)$$

$p$  is the path length from the wave plane through the origin to the scatterer given by

$$p = x_s \sin(\Theta_t) \cos(\Phi_t) + y_s \sin(\Theta_t) \sin(\Phi_t), \quad (8.66)$$

and where

$E_o$	line-of-sight field strength,
$D(\Theta_t)$	antenna voltage directivity versus elevation $\Theta_t$ ,
$\omega_o$	transmitter frequency,
$T$	transmission of direct wave: 1 = no shadowing, 0 = complete blockage,
$\sigma$	bistatic cross section of scatterer,
$R(t)$	path length between antenna and scatterer,
$\lambda$	wavelength.

This model has been shown to produce time series of received data that closely match those observed, if appropriate parameters are used. One such example is shown in Fig. 8.5 and Fig. 8.6, which respectively depict experimentally received and calculated signal level and phase for an L-Band receiver using a crossed drooping dipole antenna and moving at 24 m/s. The transmitter azimuth and elevation angles are 150° and 35°, respectively. The

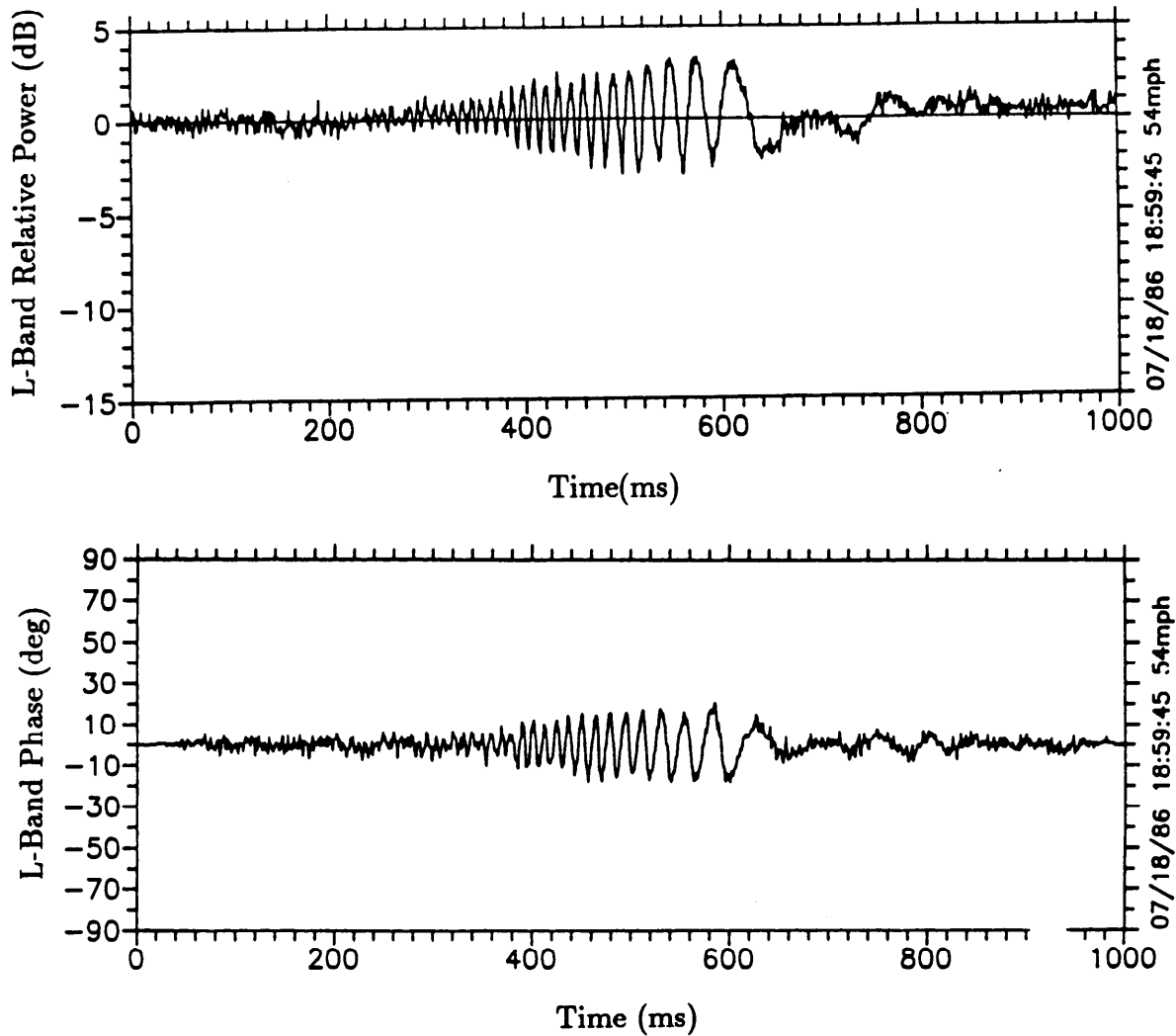


Figure 8.5: Measured L-Band signal level and phase fluctuations as a function of time relative to arbitrary reference as receiving vehicle passes by a wooded utility pole with a metal cross bar. The vehicle closest approach to the pole occurs at 540 ms.

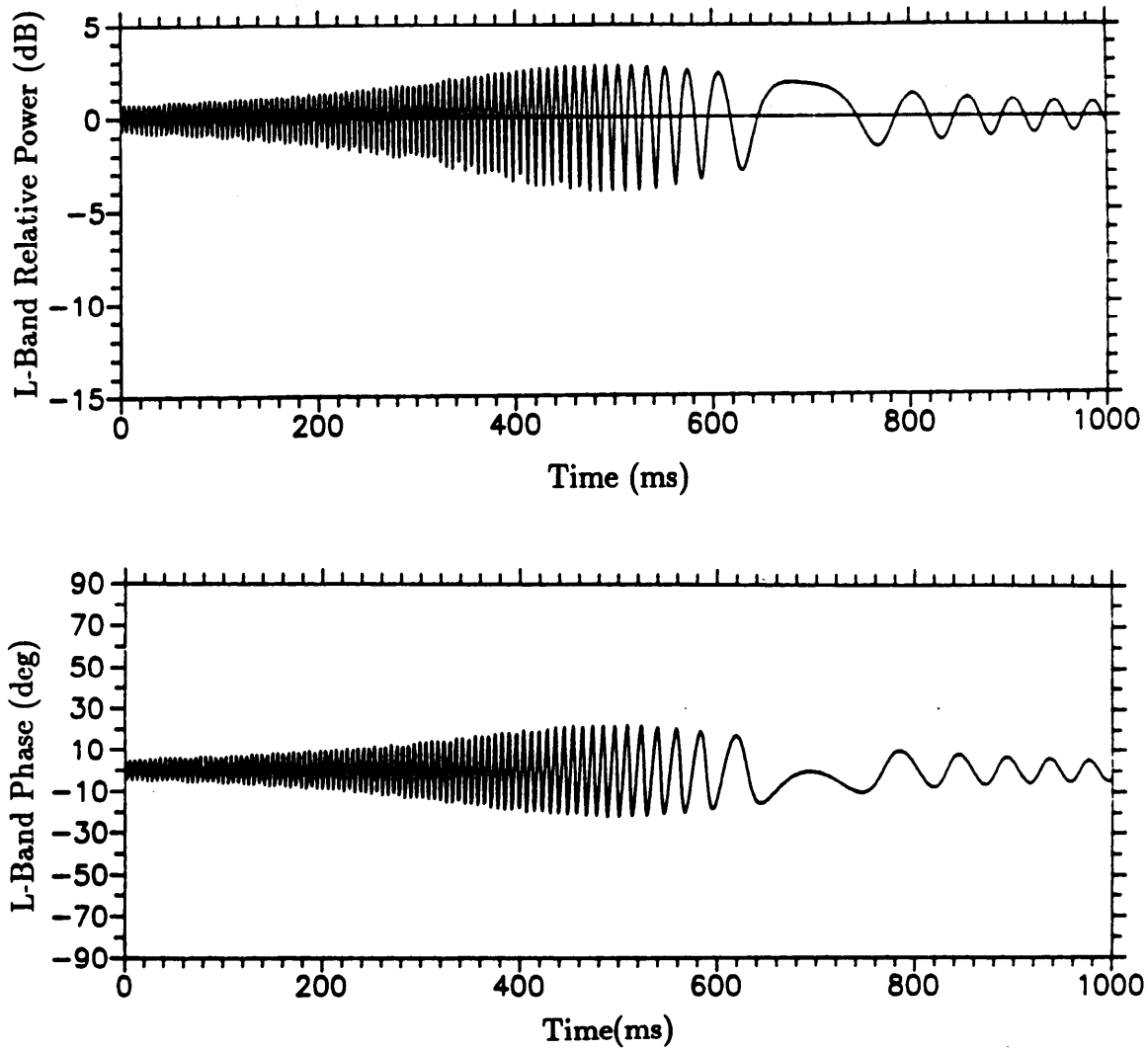


Figure 8.6: Calculated L-Band signal level and phase fluctuations as a function of time for geometry of Figure 8.5

scattering object is a wooden utility pole about 3 m to the right of and 4 m above the vehicle with a 32 m<sup>2</sup> radar cross section. The model predicts higher fluctuations before and after passing the pole, an indication that the scattering is in reality not isotropic.

Evaluating the model over a range of parameters, the following has been empirically determined:

1. The peak-to-peak fluctuations of the received signal level (dB) due to multipath vary with the inverse of the square root of the satellite elevation angle.
2. The multipath power (dB) varies as the inverse distance to the scatterer taken to the 4/3 power.
3. Assuming two frequencies (at L-Band) are simultaneously received, the rms deviation of the dB power difference between signal levels at the respective frequencies is proportional to the frequency difference. Employing this result, amplitude dispersion is found to be negligible for narrow band (bandwidth < 10 kHz) LMSS systems.

### **Fresnel Approaches to Tree Shadowing**

Several simplifying methods have been used to assess the effect of shadowing by a single tree. Modeling a tree trunk as a very long opaque strip of equal width, a diffraction pattern was obtained by LaGrone and Chapman [1961] and compared to measurements at UHF frequencies. Taking account of the tree crown, two different two-dimensional tree models have been studied, both capable of achieving rough quantitative agreement with observations of tree shadowing. One assumed a tree to be composed of a number of finite, canted opaque strips of varying width and length, representing the silhouette of a tree with branches of various sizes [Vogel and Hong, 1988]. Attenuations of up to about 12 dB were calculated at L-Band versus 8 dB at UHF. Spatial fluctuations in the shadow of the tree were found to be faster with higher signal frequency and closer proximity to the tree during a simulated drive-by scenario. The maximum fade was proportional to the logarithm of the number of limbs. In the second approach [Yoshikawa and Kagohara, 1989], the tree crown was modeled as a triangle which obscures a wedge of the first Fresnel zone. By comparisons with measurements, the results have been shown to correctly explain the average decrease of attenuation with increasing distance of the receiver from the tree.

## 8.5.2 Multiple Object Scattering Models

### Two-Dimensional Model

A two-dimensional geometric LMSS propagation model by Amoroso and Jones [1988] considered 1000 scatterers randomly distributed in an annular region with an outer radius of 2000 m and an inner radius of 400 m, corresponding to an average scatterer density of 12,000 m<sup>2</sup>/scatterer. The model has been used to correctly predict multipath Doppler spectra, both for omnidirectional and directive antennas. The simulated fading record of unmodulated carrier power for an omni-directional antenna shows unrealistic peak-to-peak variations of over 20 dB, however. This is the consequence of (1) using a two-dimensional approach, which eliminates realistic elevation angle and antenna effects, and (2) the avoidance of any scatterers in proximity to the vehicle, which in field measurements have been shown to dominate the signal variations in the absence of shadowing. The model therefore also overestimates delay spread.

### Three-Dimensional Model

An extension to the single scatterer multipath model of Vogel and Hong [1988] allows a vehicle to be driven through a region with many randomly distributed, point-source multipath scatterers [Vishakantaiah and Vogel, 1989]. The output of the drive simulator yields time series of signal amplitude and phase as well as Doppler spectra, all for user-specified conditions. These outputs, in turn, can be used to calculate system performance parameters. The simulator does not consider shadowing, and this limits its application to very low fade margin systems, where multipath fading effects determine system performance most of the time.

In order to obtain the total field at the receiver due to many scatterers, the vector sum of the constant incident field and all the scattered fields  $e$  is formed similarly to (8.63) and the relative total power and phase are calculated from

$$P'_{\text{total}} = \sqrt{\left(1 + \sum e_{\text{real}}\right)^2 + \left(\sum e_{\text{imag}}\right)^2} \quad (8.67)$$

$$\text{Phase}_{\text{total}} = \arctan \left( \frac{\sum e_{\text{imag}}}{1 + \sum e_{\text{real}}} \right) \quad (8.68)$$

where the summation includes the real or imaginary parts of each scatterer's response  $e$  to the incident wave.

The model was validated by comparing the predicted power and phase assuming a single scatterer to the results from measurements, both with similar parameters as well as by comparing the calculated power spectral density to the one expected [Clarke, 1968]. Figure 8.7 demonstrates that the model produces the correct Doppler spectrum, centered on the received carrier frequency. The shape shows the typical signature of mobile multipath propagation, a sharply bandlimited spectrum with maximum power at the edges. The frequency deviation of the scattered wave ( $\pm 120$  Hz) agrees with the value expected from the geometry. The signal level output of the model, assuming 1000 scatterers located in an annular region with radii of 400 and 2000 m, a drooping dipole antenna, and the height of the scatterers randomly distributed between 0 and 10 m, shows a peak-to-peak variation of less than 1.5 dB, a value in agreement with measurements made in locations where no scatterers are in the vicinity of the vehicle.

Similar cases to the one above, except for an outer radius of 500 m and the much higher average scatterer density of  $625 \text{ m}^2/\text{scatterer}$ , were examined with inner clearance radii from 30 to 400 m. The result demonstrates that multipath phenomena for LMSS scenarios are significant only if the scatterers are located close to the vehicle. The standard deviation of the logarithmic amplitude decreases monotonically with increasing inner clearance from 0.22 dB to 0.07 dB.

As an outgrowth of geometric modeling, it has been ascertained that when higher gain antennas are employed, the side of the road the scatterer is located influences the multipath fading [Vishakantaiah and Vogel, 1989]. For example, assuming an antenna having an  $80^\circ$  half power beamwidth in both the azimuth and elevation planes, the multipath fading was 10 dB when a simulated scatterer (e.g., a utility pole) was placed between the vehicle and the satellite. Only 1 dB multipath fading occurred when the vehicle was between the scatterer and the satellite. This diminished fading for the latter case was caused by filtering of the signal by the antenna pattern. On the other hand, when an azimuthal omni-directional antenna was used, no change in the multipath fading (e.g., 10 dB) was observed for the two cases. In an environment with many scatterers at random heights and cross sections, the reduction of the fade fluctuations arising from lower versus higher gain antennas is not as extreme, but still significant. For the case of 500 scatterers (having random heights and cross

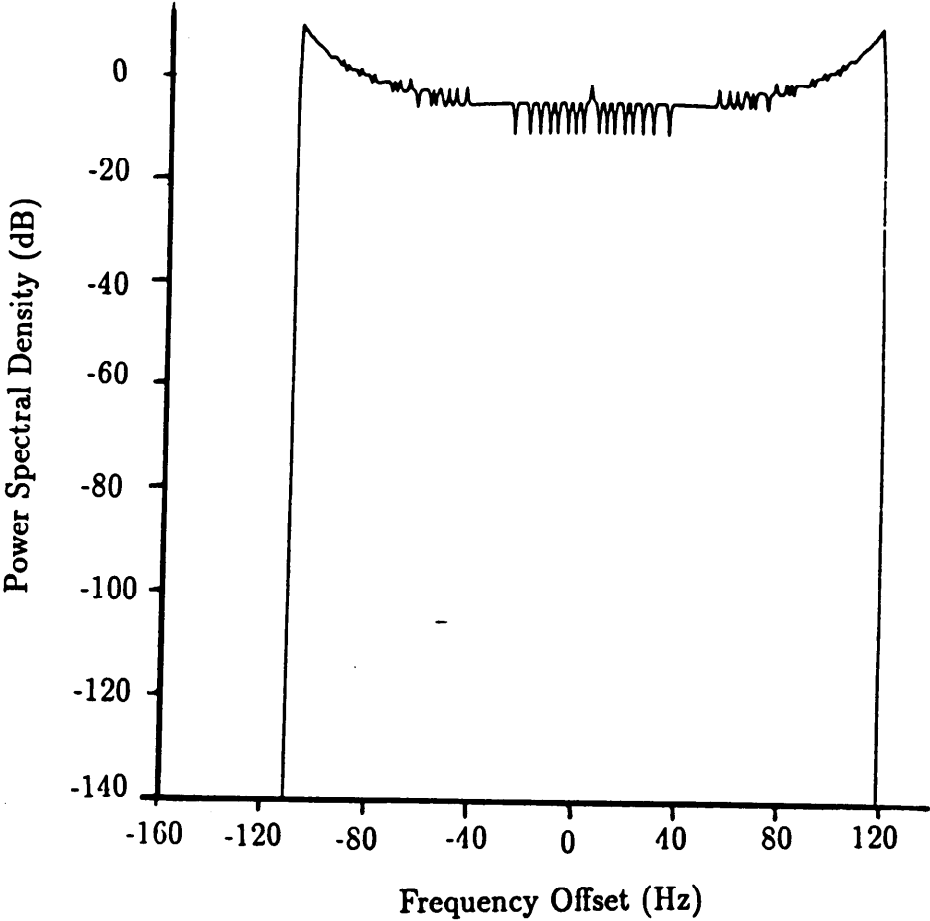


Figure 8.7: Calculated Doppler spectrum due to single multipath reflector averaged over one second, while the vehicle is driving past the scatterer.

sections ) located at distances between 10 m to 300 m, the peak-to-peak fade fluctuations were reduced from 3.6 dB (for the lower gain antenna) to 0.8 dB (for the higher gain antenna).

### Discussion

Two-dimensional simulation models overestimate multipath, because the elevation angle selectivity of the receiving antenna is neglected. Therefore they cannot be used to predict either amplitude, phase, or bandwidth effects realistically. The three-dimensional simulator demonstrates that only scatterers in the immediate vicinity of the receiver matter. As a consequence, the delay spread spectrum is narrow and has no detrimental impact on contemplated systems with channel bandwidths of 5 kHz.

Time-series produced with this model will give more realistic inputs to systems which analyze bit error performance than those based on statistical assumptions only as long as the no shadowing condition holds.

## 8.6 General Conclusions

The salient conclusions associated with model execution and development may be summarized as follows:

1. When the propagation path is unshadowed, Rician statistics apply most of the time, although the K-factor cannot strictly be assumed constant.
2. Signal variations in the clear path case are due to scattering from objects such as trees and utility poles in the vicinity of the vehicle, as weighted by the vehicle antenna pattern. Where these objects recede from or come closer to the vehicle, the K-factor decreases or increases, respectively.
3. When a single scatterer dominates, as might be the case with a utility pole, Rician statistics are no longer applicable and a geometrical analytical model must be used. This case is treated in Section 8.5.1.

4. Statistics of clear path K-factor variations have not been considered in any of the models.
5. Signal fluctuations for LMSS scenarios which are solely due to multipath scattering at path elevation angles above about  $15^\circ$  are less than 2 or 3 dB for 99% of the distance, consequently there may not be a need to have a more accurate description of "unshadowed propagation" than that given by applying Ricean multipath scattering models as given by (8.29) or by using geometric-analytic models of the type described in Section 8.5.
6. When the line-of-sight is completely blocked by continuous obstacles such as mountains, buildings, or overpasses, not enough power is contributed by multipath scattering to enable any communication through a satellite system with a commercially feasible fade margin of around 6 to 12 dB. In this case LMSS cannot be functional at all and what is required is some knowledge of the probability of blockage and its duration for specific path geometry. No separate statistical evaluations for the incidence of blockage are currently available.
7. In view of items 5 and 6, the major propagation model of interest should describe the condition of shadowing of roadside trees where complete blockage does not occur.
8. Simulation of time series of fade data for various conditions of tree shadowing is a requirement for analytically addressing fade mitigation techniques such as antenna diversity and error correction schemes.

## **8.7 Recommendations and Follow-On Efforts**

Based on the results to date as examined in this text, the following represents a list of recommendations to fill the present modeling gaps for LMSS scenarios.

1. A comparative assessment of the various statistical models described in this Chapter is recommended.
2. In the absence of 1, the authors recommend the following:

- \* Designers interested in cumulative fade distributions should employ empirical models such as ERS (Section 3.3) or the Simplified Lognormal Model (Section 8.4.5) which are derived directly from measured data.
  - \* Designers interested in fade durations and fade rates should employ Loo's model (Section 8.4.2) which appears to be the most mature.
3. Empirical models describing cumulative fade distributions should be developed from data bases associated with the following locations:
- \* regions in which elevation angles range between  $0^\circ$  to  $20^\circ$ . At angles near grazing, (e.g., northern latitudes), scintillations and refractive effects due to the troposphere may influence the fade statistics.
  - \* regions where ionospheric scintillations are prevalent such as in the tropics (e.g., geostationary satellite communications) or auroral regions for cases in which communications exist with polar orbiting satellites.
4. Systematic measurements and modeling of wideband delay spread characteristics should be executed.